MAGNETOSPHERIC MULTISCALE (MMS)
HOT PLASMA COMPOSITION ANALYZER (HPCA)

Science Algorithms and User Manual

MARCH 10, 2016

SwRI® Project 10160

Document No. 10160.13-MMS-HPCA_SCI_ALG_UM

Rev 20160310 Chg 0

Contract # (To be found)

Pre-Signature/Pre-Document Control

Prepared by

Roman Gomez

SOUTHWEST RESEARCH INSTITUTE®

Space Science and Engineering Division

6220 Culebra Road, San Antonio, Texas 78228-0510

(210) 684-5111 • FAX (210) 647-4325

MAGNETOSPHERIC MULTISCALE (MMS)
HOT PLASMA COMPOSITION ANALYZER (HPCA)

Science Algorithms and User Manual

SwRI® Project 10160

Document No. 10160.13-MMS-HPCA_SCI_ALG_UM

Rev 20160310 Chg 0

Contract # (To be found)

Prepared by: Roman Gomez March 2016

Approved by: _____ Date:_____

Stephen Fuselier, MMS HPCA Principal Investigator

Approved by: _____ Date:_____

Roman Gomez, MMS HPCA Scientist

Approved by: _____ Date:_____

Judith Furman, MMS HPCA Project Manager

Released by: _____ Date:_____

, SwRI Project CM

Space Science and Engineering Division

Southwest Research Institute

P. O. Drawer 28510

6220 Culebra Road

San Antonio, Texas 78228-0510

(210) 684-5111

TABLE OF CONTENTS

1. SCOPE 4

2. Instrument Description 4

2.1 ESA 4
2.2 TOF 5
2.2.1 Determining Doubly Charged Oxygen counts 7
2.3 Coordinates 9
2.3.1 ESA Voltages -Energy 9
2.3.2 Start Anodes - Elevation 10
2.3.3 Spacecraft Rotation - Azimuth 14
2.4 Geometric Factor 18
2.4.1 Effective Area 18
2.4.2 Integrated Energy-Azimuth Response, $<\Delta E/E\ \Delta\alpha>$ 21
2.4.3 Geometric Factor for HPCA 21

3. Data Products 21

3.1 LEVEL 0 - Counts 22
3.2 LEVEL 1a -Flux 22
3.3 LEVEL 1b -$f_s(v)$ 22
3.4 Plasma Distribution Moments 24
3.4.1 Ion number density (n_s) 24
3.4.2 Ion Bulk Velocity (u_s) 25
3.4.3 Scalar Ion Temperature 25
3.4.4 Ion Temperature Tensor 26

4. Data Products with RF 31

5. Level 2 Data Products: In the magnetic field reference frame 31

5.1 Bulk velocity in the Magnetic Field Frame 32
5.2 f(v) in the Field aligned coordinates 32

6. Appendix 1- Re-evaluation of Effective Area based on Instrument Flux Measurements 35

7. Appendix-2 Table of HPCA Specific Level 2 Parameter Values and units 38

1. SCOPE

The purpose of this document is to describe the operational principles of the MMS-HPCA (Magnetospheric Multi-Scale - Hot Plasma Composition Analyzer), and to provide the algorithms and quantities needed to convert acquired counts to physical units.

2. Instrument Description

MMS-HPCA measures the energy and composition of magnetospheric plasmas with an electrostatic energy analyzer (ESA) which is optically coupled to a carbon-foil based Time-of-flight (TOF) section. The following sections address the operational principles of both ion-optical components.

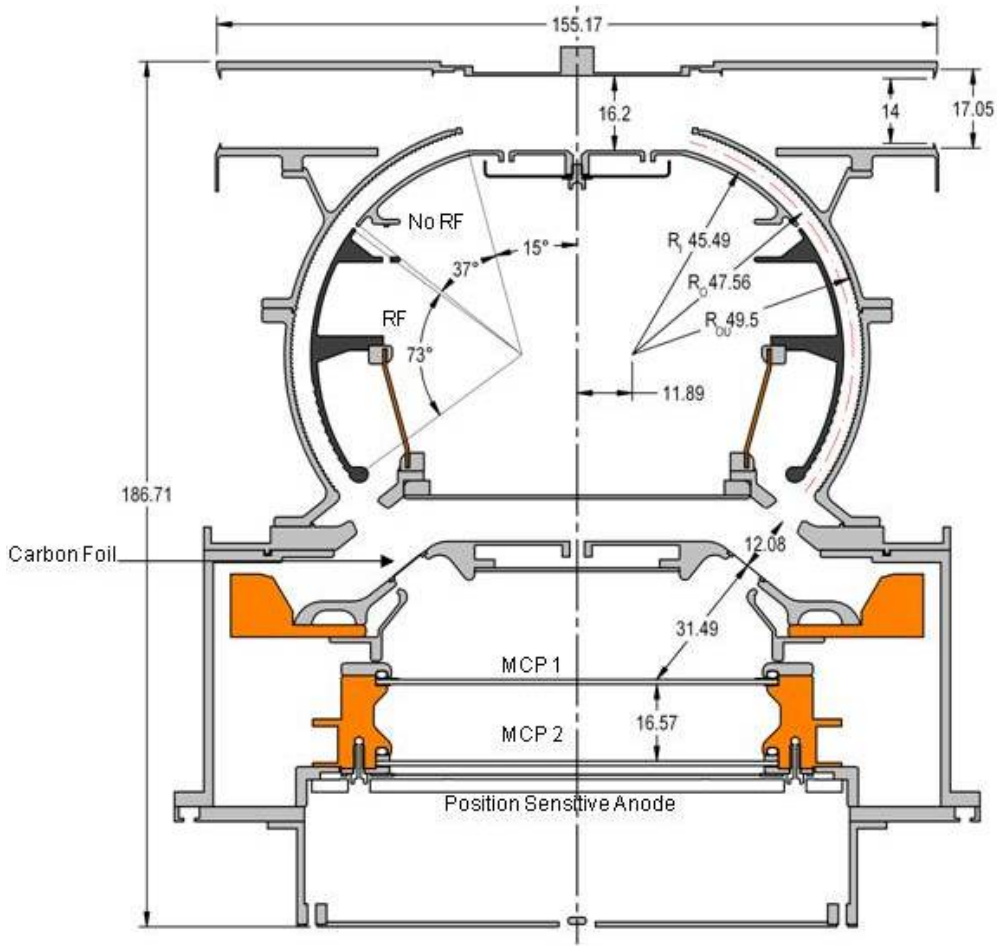

Figure 1. HPCA Dimensions

2.1 ESA

HPCA scans plasmas in the energy range 1 eV - 40 keV using an ESA with inner and outer conducting electrode radii of R_1 = 45.5 mm and R_2 = 49.5 mm. These conducting electrodes are more commonly called ESA plates. The ESA bending angle of $\gamma = 125.0°$ insures that UV photons from the sun do not have a direct path to the particle sensitive microchannel plates (MCPs), which can cause excessive background during data acquisition. ESAs deflect the paths of charged particles in a specified energy range set by the plate spacing ($\Delta R = R_2 - R_1$),the average plate radius, $R_0 = (R2 + R1)/2$, and the voltage difference between the plates, $\Delta V = V_2 - V_1$; where $V_{1/2}$ is the voltage applied to the inner/outer plate. The analyzer geometry determines the energy and angular resolutions as well as the ESA's analyzer constant, *k*; a constant of proportionality between the ESA plate voltage difference and central energy of the acceptance passband. This energy is set according to (1):

$$E = k\Delta V \tag{1}$$

The analyzer constants of all four HPCA flight models were determined from calibration results at eight energies; 98 eV, 312 eV, 512 eV, 995 eV, 3159 eV, 10059 eV, 19525 eV, and 32040 eV. Their *k*'s are shown in the next table.

Table 1: HPCA Flight Model Analyzer Constants

HPCA Flight Model	Analyzer Constant - *k*[eV/V]	Uncertainty (+/-) [eV/V]
1	5.42	0.01
2	5.42	0.01
3	5.39	0.04
4	5.39	0.02

During operation, voltage is applied to the inner ESA plate of HPCA; the outer plate is held at spacecraft ground, so ΔV is just the voltage on the inner plate; $\Delta V = V_1$.

2.2 TOF

Particles that are permitted through the ESA plates, exit and are post-accelerated by a 15 kV potential on their way to one of sixteen thin carbon foils placed at the entrance to the TOF section. Ion impacts cause secondary electron emission from both foil surfaces. In the vast majority of interactions, ions assume a neutral charge state through charge exchange with the foil. Electrons emitted from the bottom surface facing the TOF section are accelerated, and focused with steering electrodes to MCP1 (see Figure 1), where their signals are amplified by over 6 orders of magnitude. These amplified signals then impact one of the sixteen elevation-start (β) pads shown in Figure 2.

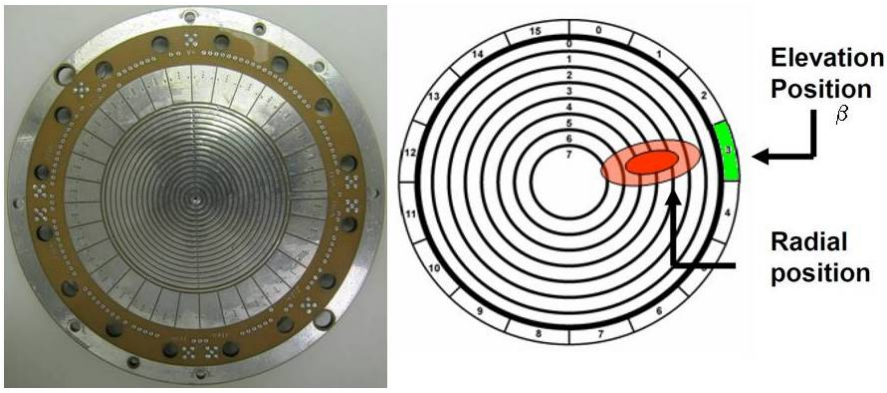

Figure 2. HPCA Position Sensitive Anode. At left, the anode with 16 elevation-start pads and 16 concentric stop rings. At right, the operation of the anode with respect to elevation detection, and flight distance correction.

Electron transit times within the TOF region are short (< 5.0 ns). By comparison, the transit time for a proton at 45 keV (60 keV with the 15 kV post acceleration), the highest energy scanned by HPCA, is > 9.0 ns. Because of this time difference, electron signals at the pads are used to signal the start of a time-of-flight measurement (TOF).

Ion signals impact MCP1 above the concentric array of sixteen anode rings (Figure 2). The rings are used to correct for the change in the particle flight path due to angular scattering within the foil. The ion signals are the stop signals for a TOF measurement. The ion time of flight (TOF) in this region has the analytical form (2):

$$TOF = \frac{d}{\sqrt{\frac{2E}{m}}} \qquad \textbf{(2)}$$

where d is the length of the nominal flight path (3.15 cm), E the ion energy in eV, and m the ion mass-to-charge ratios provided in Table 2. HPCA measures ion TOF from 0 ns to 256 ns in 0.5 ns resolution (512 TOF channels).

Table 2: HPCA Species Mass-to-Charge Ratios

Ion Species	Mass-to-Charge Ratio (M/q) [AMU/e]	Mass-to-Charge Ratio [eV/c^2 e]
H^+	1	0.939494061e9
He^{++} (alpha particle)	2	1.87898812e9

He^{+}	4	3.75797624e9
O^{++} (Doubly Charged Oxygen)	8	7.51595249e9
O^{+}	16	15.031905e9

HPCA's dual delay line, and the uncertainty in the energy loss from foil straggling makes an analytical fit with (1) very difficult. Instead, energy dependent TOF measurements made during calibration are used to assign channels of the TOF spectrum to specific ions as shown in Figure 3:

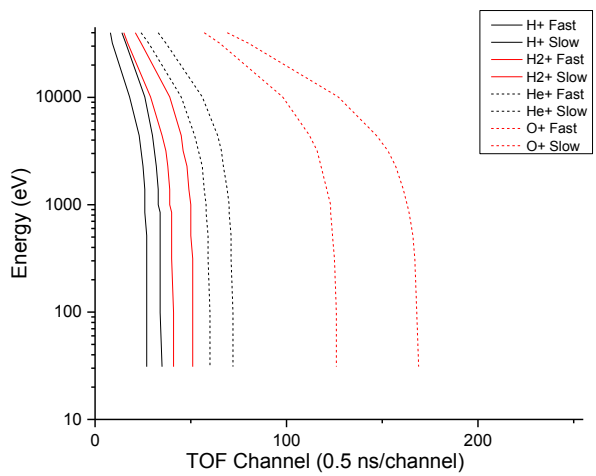

Figure 3. HPCA TOF Channel Assignment from calibration

As shown in Figure 3, ions of a given mass (e.g. H^{+} ,1 AMU) will populate a specific range of TOF channels, at a given post foil energy. The measured responses at eight energies are used to interpolate, and extrapolate the responses at other energies. Note that O^{2+} bins are not shown in Figure 3. This is because getting these counts requires special treatment of the background ion count product. This treatment will be discussed shortly. In addition to energy and composition, the HPCA's construction allows surveys of the plasma phase space with high resolution in solid angle. These resolutions will be discussed in later sections. But first we will discuss the technique used to get O^{2+} counts from the background ion count product.

2.2.1 Determining Doubly Charged Oxygen counts

The basic HPCA data product is an array of counts for 5 ion species, at 63 energies, for each elevation anode (16). Sixteen basic products, also called azimuths, are acquired every 10 seconds; half a spacecraft spin period nominally has 16 azimuths. The five ion species are protons (H^+), alpha particles (He^{2+}), helium ions (He^+), singly charged Oxygen (O^+), and background counts. The background counts are acquired in the TOF bin range between the slowest helium, and fastest singly charged oxygen ion at each energy (see Figure 3). These bin ranges contain ranges where the TOFs of doubly charged oxygen ions (O^{2+}) can be counted as well. To get these counts out of the background counts requires manipulation of the background product. The technique will be described here.

To start, we perform the following operation on the background ion counts:

$$\left[\frac{noise}{bin}\right]_\beta = \sum_{E=0}^{63} N_{E,\beta,Background} \Big/ \sum_{E=0}^{63} \left[N(bins)_{background}\right]_E \qquad \textbf{(3)}$$

which is based on the following assumptions:

1. The background is independent of energy
2. Background can be influenced by the gain of individual detector pixels
3. Ion species that can populate the background bins are in low concentration in most plasmas
4. HPCA, with its double coincidence detection scheme, greatly reduces spurious noise

In (3) the variable $[N(bins)_{background}]$ is the number of bins, at respective energies, over which the background counts are accumulated. Note that the sum is carried out over energy only, which addresses assumptions 1 and 2 in the list. [Noise/Bin] is then a 16 element array. Once computed, it is used to determine the corrected ion flux.

The ion flux at energy E in counts cm^{-2} sr^{-1} eV^{-1} is determined from:

$$J_{E,\beta,s} = \frac{C_{E,\beta,s}}{G(E)\left(\frac{E}{q}\right)_s} \qquad \textbf{(4)}$$

Where G(E) is the energy specific geometric factor of the instrument at E. However, before computing $J_{E,\beta,s}$ the corrected ion counts must be calculated by subtracting the $[noise/bin]_\beta$ value as shown:

$$C_{E,\beta,s} = \left(N_{E,\beta,s} - N(bins)_{s,E} \times \left[\frac{noise}{bin}\right]_\beta\right) \Big/ \Delta\tau \qquad \textbf{(5)}$$

Where $N(bins)_s$ is the number of bins, at energy E, for which ion species *s* counts are accumulated. The doubly charged oxygen product comes from this when the background counter is operated upon as shown here:

$$C_{E,\square,O++} = \left(N_{E,\square,background} - N(bins)_{background,E} \times \left[\frac{noise}{bin}\right]_{\beta}\right) \Big/ \Delta\tau \qquad \textbf{(6)}$$

Then the O++ flux is computed from:

$$J_{E,\beta,O++} = \frac{C_{E,\beta,O++}}{G(E)\left(\frac{E}{q}\right)_s} \qquad \textbf{(7)}$$

2.3 Coordinates

HPCA bins the phase-space of a plasma under observation into one dimension of energy, two of angles, and five ion masses as shown in Table 3. Also included in the table are the HPCA parameters which control the dimensions, the dimensional symbols, the indices of these parameters and their ranges.

Table 3. HPCA Phase Space Scanning Dimensions

Dimension	Mediating Parameter	Symbol	Index	Index Values
Energy	ESA Voltage	*E*	*i*	0-62 (63 is flyback)
Elevation	Start Anode	*β*	*j*	0-15
Azimuth	Spin-Energy Sweep	*α*	*k*	0-15
Ion Species	Time-of-Flight Binning	*m*	*s*	0-4 : 0 = H^+; 1 = He^{2+}; 2 = He^+; 3 = O^+, 4 = background

Each of these dimensions, and how they are sampled, are discussed below.

2.3.1 ESA Voltages -Energy

During normal operation, the energy range (1 eV - 40 keV) is scanned by using table of logarithmically spaced ESA voltages. Regardless of the instrument sampling mode (slow survey, fast survey, or burst - these modes will be discussed shortly) HPCA scans this energy range in 625 ms, including ramp and sample times. The sample time at each energy is 8.950 ms. There are 63 energy sample steps in the HPCA table; the 64th is a flyback step which sets the inner plate voltage to spacecraft ground, making ΔV = 0 V. The energy at each step is determined using (1). The voltages are set according to the voltage sweep tables supplied to each instrument.

2.3.2 Start Anodes - Elevation

At each voltage step, V_i, HPCA captures 16 individual TOF measurements; one for each elevation anode. Because of the clocking of the microchannel plates and the bias angle of their channels, there is signal gain variation between adjacent anodes which requires specific corrections. This effect is plainly evident in an elevation scan about the instrument aperture (shown in Figure 4).

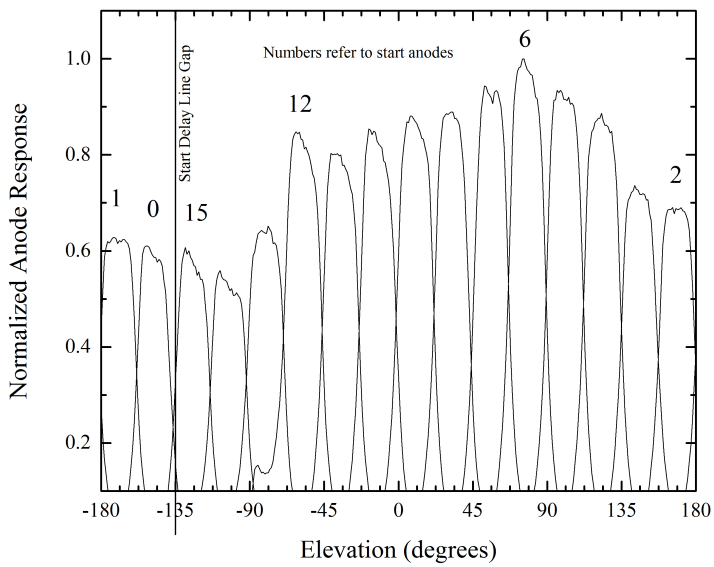

Figure 4: HPCA Flight Model 4 (FM4) Elevation and Anode Gain Response

In addition, as shown in Figure 1, HPCA's top-hat ESA configuration means that ions are accepted across the instrument's symmetry plane and their signals are registered on the anode that sits opposite the location of ion entry in the instrument aperture. The anode, and flight model specific, gain corrections are included in Table 4.

Table 4: Anode Specific gain correction factors for HPCA flight models 1-4

Anode	FM1	FM2	FM3	FM4
0	1.69	1.96	1.58	1.63
1	1.30	1.58	1.35	1.47

2	1.39	1.52	1.42	1.42
3	1.30	1.36	1.30	1.31
4	1.20	1.16	1.23	1.11
5	1.09	1.21	1.07	1.04
6	1.05	1.14	1.00	1.00
7	1.02	1.00	1.09	1.09
8	1.04	1.02	1.05	1.14
9	1.00	1.04	1.06	1.06
10	1.06	1.09	1.13	1.13
11	1.10	1.12	1.07	1.16
12	1.07	1.14	1.04	1.05
13	1.29	1.23	1.28	1.33
14	1.65	1.41	1.38	1.65
15	1.70	1.67	1.64	1.68

The elevation anode locations (yellow numbers on pads) and their look directions (black numbers within outer dotted circle in the figure) are shown in Figure 4.

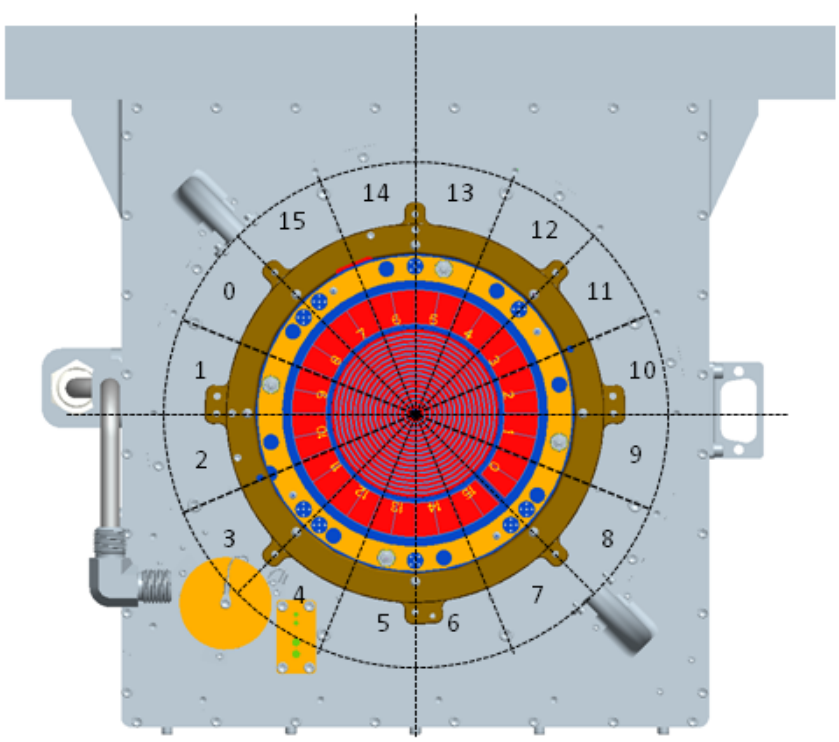

Figure 5. HPCA Start anode arrangement and Field-of-View (FOV) sectors for instrument mounted on MMS Spacecraft.

The nominal centers of ion arrival directions for the instrument mounted on the spacecraft, are supplied in Table 5. The top-hat ESA configuration allows eight anodes to view one azimuthal direction, while the other eight view azimuthal space that is angularly displaced by 180°. The centers of the 16 anodes trace out circles of constant elevation as the spacecraft spins. As shown in Figure 5, and as indicated in Table 5, the anodes sample elevation space in its entirety; $0° \leq \beta \leq 180°$.

Table 5. HPCA start nominal anode look directions

Anode	Centroid β View (°) - Elevation
0	123.75
1	101.25
2	78.75
3	56.25
4	33.75
5	11.25
6	11.25
7	33.75
8	56.25
9	78.75
10	101.25
11	123.75
12	146.25
13	168.75
14	168.75
15	146.25

The FWHM field of view (FOV) is averaged over 16 anodes and 63 energies. This value, which is unique to each flight model, is provided in Table 6 along with the measured uncertainty in this parameter.

Table 6. HPCA Anode-Elevation response

Flight Model	Δβ FWHM [°]	Δβ FWHM-Error [°]
1	24.0	0.7
2	24.8	0.7
3	24.1	0.7
4	23.8	0.7

The values in Table 5 and Table 6 are important for determining the moments of the plasma distribution function, f(**v**). Computing these moments is a subject of later sections.

In addition to gain, a correction for sky coverage is required in the calculations. Each HPCA anode covers approximately 24° or 0.419 radians (Table 6) in elevation. Anode centers are separated by 22.5° as shown in Table 5 (or 1.07 steradians). Per full energy sweep at a spin rate of 3 Hz, 11.25° of azimuthal angle space is covered. However, as shown in Figure 6, there is an excess of 7° (0.122 radians) in this field-of-view. Thus each anode sees 0.133 steradians of solid angle space at this spin rate. This gives an overestimation in particle flux for a given phase-space parcel, which leads to errors in f(**v**) and moment calculations. The following table (Table 7) provides the correction factors to prevent this error.

Table 7: HPCA Solid Angle Space Correction Factors

Anode	Solid Angle Space Correction
0	2.09
1	1.78
2	1.78
3	2.09
4	3.13
5	8.93
6	8.93
7	3.13
8	2.09
9	1.78

10	1.78
11	2.09
12	3.13
13	8.93
14	8.93
15	3.13

The next section addresses how the azimuth components of the plasma distribution are acquired.

2.3.3 Spacecraft Rotation - Azimuth

MMS has a nominal a spin period of 20 seconds. HPCA has a 90° azimuthal offset, relative to the DSS sun pulse detector, for elevation anodes 14, 15, 0, 1, 2, 3, 4, and 5, and 270° for the remaining anodes. Because of HPCA's elevation FOV and top-hat construction it sees 4π steradians (full sky view) in half a spacecraft spin. In 20 seconds, HPCA will sweep the entire energy range of 1eV - 40 keV 16 times. While the uniform sample time at each energy step was already discussed in section 2.3.1, the dwell times were not. These time steps are not uniform, and increase with increasing voltage magnitude. Because of these steps the azimuthal look directions vary between adjacent steps. HPCA also has an inherent FWHM azimuthal resolution of 7.0°. This is plotted in Figure 6.

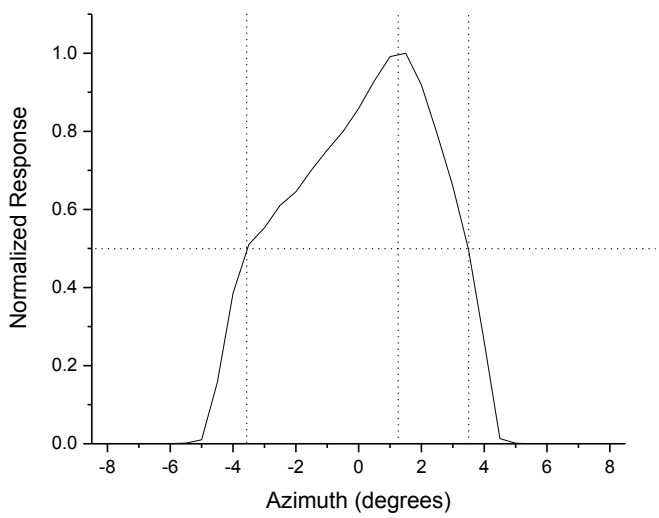

Figure 6. HPCA Azimuth (α) response

The horizontal line in Figure 6 indicates the half-maximum response. The vertical lines, from left to right are the negative half-maximum limit, the center response, and the positive half-maximum limit. As seen here, HPCAs FWHM response is for all intents symmetric. However, the center response is offset by +1°.

This angular response is swept through 11.25° in one energy sweep. In the graphs shown below(Figure 7) the sequence of energies and α angles are shown as a function time, assuming at HPCA starts at Sweep Time = 0 on the x-axis. The first α-look direction is 0.275° at an energy of 1.34 eV ($V_{i=0}$ = -0.2477 V), and the last acquisition at $V_{i = 62}$ = 6936 V (37454.4 eV) occurs when the α-look is 10.940°. At the end of the sweep 625 ms later α = 11.25°, and $V_{i = 63}$ = 0 V.

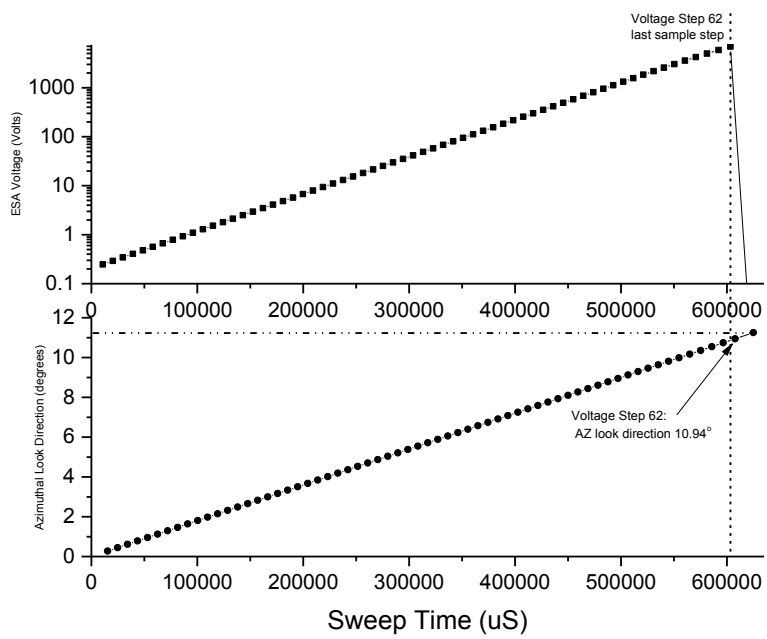

Figure 7. HPCA energy sweeping and azimuth look direction

The α-look directions, calculated at the center of each energy acquisition step, are in Table 8.

Table 8. HPCA azimuthal arrival directions in 1 energy sweep

Energy Step	α-look (°) Anodes 14, 15, 0-5	α-look (°) Anodes 6-13
0	0	180
1	0.17	180.17
2	0.341	180.341
3	0.511	180.511

4	0.681	180.681
5	0.851	180.851
6	1.021	181.021
7	1.191	181.191
8	1.361	181.361
9	1.531	181.531
10	1.701	181.701
11	1.871	181.871
12	2.042	182.042
13	2.212	182.212
14	2.382	182.382
15	2.552	182.552
16	2.722	182.722
17	2.892	182.892
18	3.062	183.062
19	3.232	183.232
20	3.402	183.402
21	3.572	183.572
22	3.743	183.743
23	3.913	183.913
24	4.083	184.083
25	4.253	184.253
26	4.423	184.423
27	4.593	184.593
28	4.763	184.763
29	4.933	184.933
30	5.103	185.103
31	5.273	185.273
32	5.444	185.444
33	5.614	185.614

34	5.784	185.784
35	5.954	185.954
36	6.124	186.124
37	6.294	186.294
38	6.464	186.464
39	6.634	186.634
40	6.804	186.804
41	6.974	186.974
42	7.145	187.145
43	7.315	187.315
44	7.485	187.485
45	7.655	187.655
46	7.825	187.825
47	7.995	187.995
48	8.165	188.165
49	8.335	188.335
50	8.505	188.505
51	8.675	188.675
52	8.846	188.846
53	9.016	189.016
54	9.187	189.187
55	9.36	189.36
56	9.535	189.535
57	9.713	189.713
58	9.894	189.894
59	10.079	190.079
60	10.269	190.269
61	10.464	190.464
62	10.666	190.666
63	10.975	190.975

Note: The values in this table are provided for diagnostic purposes. Whether they will be used to compute moments is still under consideration.

The values shown in Table 8 were calculated using a spacecraft spin period of 20 seconds. If this is not the case then the general expression for the HPCA azimuthal look direction is:

	$\alpha_{HPCA} = \frac{121^\circ \pi}{180^\circ} + \frac{2\pi}{\tau_{sc}} \left(\Delta t + \frac{\tau_{acq}}{2} + k \times \tau_{acq}\right)$	**(8)**

where in (8) τ_{sc} is the spacecraft spin period, or the time between two sequential sun pulses. Δt is the time that has passed since the most recent sun pulse. τ_{acq} is the acquisition time for a full energy sweep (0.625 s) Recall that (8) applies to elevation anodes 14, 15, and 0-5; for anodes 6-13 add π radians, up to a maximum of 2π.

2.4 Geometric Factor

The convolved differential field-of-views (FOVs) in energy and solid angle space for a single HPCA elevation pixel is called its geometric factor; denoted G. G depends on energy (i) and on a pixel dependent gain factor (already discussed in Table 4). In this case G becomes $G_{i,j}$ and it is expressed as (9).

$$G_{i,j} = A_{eff}\left(E_i, \beta_j, \alpha_k\right) \left\langle \frac{\Delta E}{E} \Delta\alpha \right\rangle \Delta\beta \qquad \textbf{(9)}$$

where A_{eff}, is an area external to the instrument which corresponds to the jth start pixel's flux sensitivity; this also includes detector efficiencies. Also included are the integrated energy-azimuth response , $\langle \Delta E/E \, \Delta\alpha \rangle$, which is a differential quantity that is unique to the instrument and is energy independent. $\Delta\beta$ is the FWHM elevation response of the HPCA flight model given in Table 6. We will first discuss A_{eff}.

2.4.1 Effective Area

The A_{eff} of an elevation anode, as shown in (10), is a sensitive external area, A_0, divided by the gain factor of the respective anode, g_j (Table 4).

$$A_{eff} = \frac{A_0(E_i)}{g_j} \qquad \textbf{(10)}$$

The anode is with the largest response is assigned a g_j value of 1. A_0 is computed with the calibration data from this anode. The A_0 values of all four FMs, which are energy dependent, are provided in Table 9.

Table 9. HPCA A_0's at energy

Voltage Step	A_0 FM 1	A_0 FM 2	A_0 FM 3	A_0 FM 4

(i)	(cm^2)	(cm^2)	(cm^2)	(cm^2)
0	0.025	0.028	0.047	0.047
1	0.025	0.029	0.047	0.047
2	0.026	0.029	0.048	0.048
3	0.026	0.030	0.049	0.049
4	0.026	0.030	0.050	0.050
5	0.027	0.030	0.051	0.051
6	0.027	0.031	0.052	0.051
7	0.028	0.032	0.052	0.052
8	0.028	0.032	0.053	0.053
9	0.029	0.033	0.054	0.054
10	0.029	0.033	0.055	0.055
11	0.030	0.034	0.056	0.056
12	0.030	0.034	0.057	0.057
13	0.031	0.035	0.058	0.058
14	0.031	0.035	0.059	0.059
15	0.032	0.036	0.060	0.060
16	0.032	0.037	0.061	0.061
17	0.033	0.037	0.062	0.062
18	0.033	0.038	0.063	0.063
19	0.034	0.038	0.064	0.064
20	0.035	0.039	0.065	0.065
21	0.035	0.040	0.066	0.066
22	0.036	0.040	0.067	0.067
23	0.036	0.041	0.068	0.068
24	0.037	0.042	0.069	0.069
25	0.037	0.042	0.071	0.070
26	0.038	0.043	0.072	0.072
27	0.039	0.044	0.073	0.073
28	0.039	0.045	0.074	0.074

29	0.040	0.045	0.075	0.075
30	0.041	0.046	0.077	0.076
31	0.041	0.047	0.078	0.078
32	0.042	0.048	0.079	0.079
33	0.043	0.048	0.080	0.080
34	0.043	0.049	0.082	0.082
35	0.044	0.050	0.083	0.083
36	0.045	0.051	0.085	0.084
37	0.046	0.052	0.086	0.086
38	0.046	0.053	0.087	0.087
39	0.047	0.053	0.089	0.089
40	0.048	0.054	0.090	0.090
41	0.049	0.055	0.092	0.092
42	0.050	0.056	0.093	0.093
43	0.050	0.057	0.095	0.095
44	0.051	0.058	0.096	0.096
45	0.052	0.059	0.098	0.098
46	0.053	0.060	0.100	0.100
47	0.054	0.061	0.101	0.101
48	0.055	0.062	0.103	0.103
49	0.056	0.063	0.105	0.105
50	0.057	0.064	0.107	0.106
51	0.058	0.065	0.108	0.108
52	0.059	0.066	0.110	0.110
53	0.060	0.067	0.112	0.112
54	0.060	0.068	0.114	0.114
55	0.062	0.070	0.116	0.116
56	0.063	0.071	0.118	0.117
57	0.064	0.072	0.120	0.119
58	0.068	0.077	0.127	0.127

59	0.066	0.074	0.124	0.123
60	0.063	0.072	0.119	0.119
61	0.061	0.069	0.114	0.114
62	0.057	0.065	0.108	0.108
63	0.000	0.000	0.000	0.000

With the values of A_0 and anode specific gain g_j discussed, we now turn to the integrated response, <ΔE/E Δα>.

2.4.2 Integrated Energy-Azimuth Response, <ΔE/E Δα>

The integrated response describes the instantaneous phase space view of HPCA, when it is tuned to center passband energy E_i, as described in (1) and in section 2.3.1. This response is a consequence of the ESA geometry; it is unique, and independent of energy. The values for FMs 1-4 are provided in Table 4.

Table 10. <ΔE/E Δα> for HPCA FMs 1-4

Flight Model	<ΔE/E Δα> [eV/eV rads]
FM1	9.68E-03
FM2	8.27E-03
FM3	7.63E-03
FM4	7.46E-03

These values are determined from the average instrument responses at all eight calibration energies.

2.4.3 Geometric Factor for HPCA

With the values included in the tables, the expression for geometric factor is now (11):

$$G_{i,j} = \frac{A_0(E_i)}{g_j} \langle \frac{\Delta E}{E} \Delta\alpha \rangle \; \Delta\beta \frac{\pi}{180^\circ} \qquad \textbf{(11)}$$

where the appropriate values have now been inserted for A_0, g_j and Δβ. The π/180° conversion is necessary because Δβ is provided in degrees in Table 6. With these values, it is now possible to compute particle flux, the velocity distribution function, f(**v**), and other data products. These will be covered in the following section.

3. Data Products

HPCA data products are based primarily on a single energy sweep of 625 ms. For a single energy, the acquisition product is 16 β x 1 α x 4 s = 64 ion count rates. We begin the discussion of data conversions with this product

3.1 LEVEL 0 - Counts

The counts acquired in a single energy sweep gives 63 values of the single acquisition product. At each (E,β,α) combination, the count rate of ion species s is (12):

$$C_{i,j,k,s} = \frac{N_s(E_i, \beta_j, \alpha_k)}{\Delta\tau} \quad \textbf{(12)}$$

where N_s is the number of ions counted at energy i, on anode j, in azimuth k, in the acquisition period Δτ. This data product requires no processing; it is a raw count measurement.

3.2 LEVEL 1a -Flux

The next data product to compute is the ion flux of species s. This is the first derived data product. The raw counts are converted to flux in units of (e eV^{-1} sr cm^{-2} s^{-1}). The conversion from count rate to flux is (13):

$$J_{i,j,k,s} = \frac{C_{i,j,k,s}}{G_j(E_i)\left(\frac{E_i}{q}\right)_s} \quad \textbf{(13)}$$

In this equation, the term in the numerator $(E_i/q)_s$ is the mass-to-charge ratio for the ion species s: For singly charged ion species (H^+, He^+, O^+), this is equal to $(E_i/e)_s$ where e is the elementary charge ($e=1.602x10^{-19}$ coulombs); it is $(E_i/2e)_s$ for doubly charged ions (He^{2+}, O^{2+}).

3.3 LEVEL 1b -$f_s(v)$

The next data product to determine is the velocity distribution function of the ion species s. This product depends on the acquisition mode of the instrument which determines data decimation and timing. There are three HPCA survey modes: slow survey, fast survey, and burst. The decimations and timing are shown in the table below.

Mode	α	β	Energies	Full Sampling Period	f(v) dimensions
Slow Survey	8	8	16	3.5 Spins (70 seconds)	5 species x 16α x 16β x 64E
Fast Survey	8	8	16	1/2 Spin (10 seconds)	5 species x 16α x 16β x 64E

Burst	16	16	64	1/2 Spin (10 Seconds)	5 species x 16α x 16β x 64E

As shown in the table, the only acquisition mode that has data in full resolution is Burst mode. Slow and Fast Survey modes have the same decimation, but are sampled at different cadences. However, moment calculations will always be carried out with an array having the burst dimensions. Because of this computing the velocity distribution function is not straightforward and it requires some discussion. In fast and slow survey the 4 steps are co-added in energy, which means that the value is the sum of 4 smaller steps. To get this to a proper count rate this value should be divided by 4 times the acquisition time, Δτ. For decimation in elevation the new values for each are divided by two, since they are summed over two elevation bins. This process is shown in the next Figure.

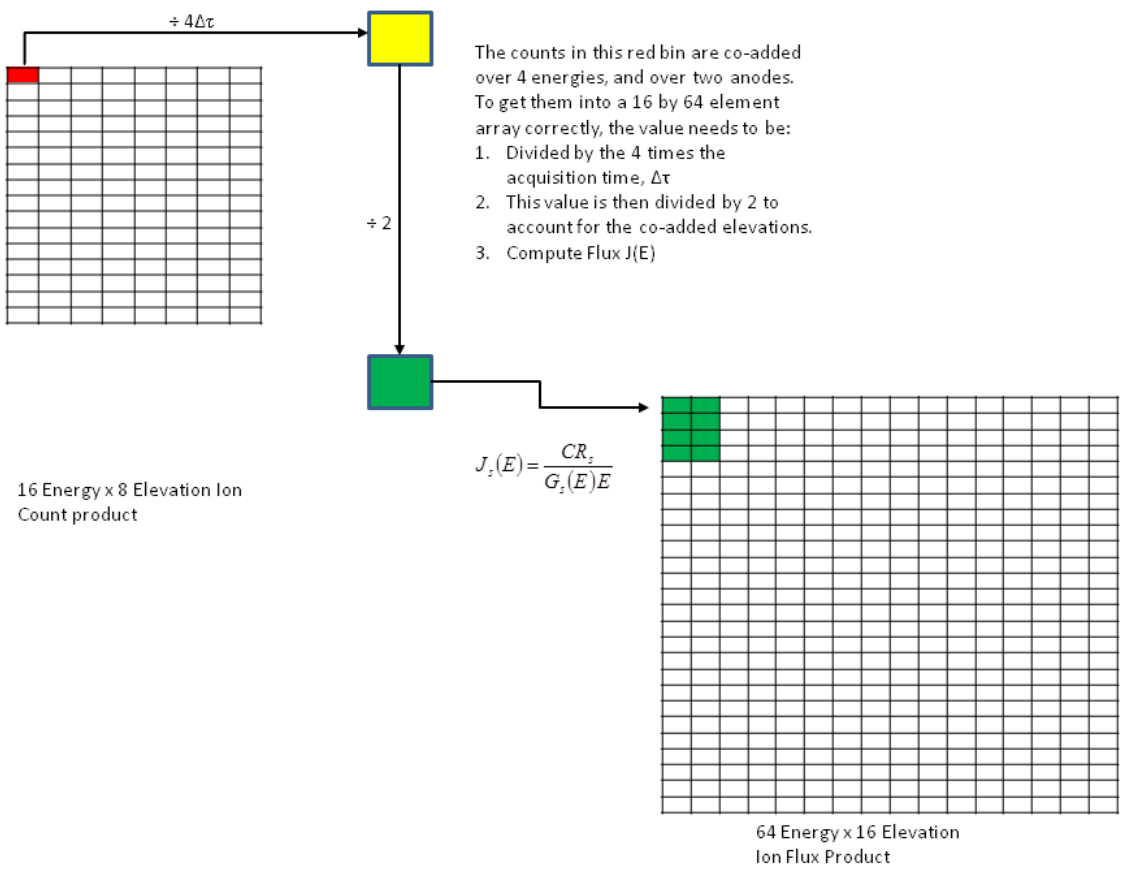

Figure 8: Correcting Counts for Decimation before converting to flux

Up to this point, the flux is corrected for energy, and elevation decimations. It still needs to be corrected for the decimation in azimuth. This calculation only affects $f_s(v)$. Slow and fast survey azimuths are co-added, resulting in 8 azimuths per full sky view. Each of the 8 flux measurements need to be divided by 2 and made into 16 flux measurements. Once done, $f_s(v)$ can be determined as shown in (14):

$$f_{i,j,k,s} = \frac{J_{i,j,k,s}}{2E_i} m_s^2 \qquad \textbf{(14)}$$

where $f_{i,j,k}$ is the velocity distribution function for each ion species s, in $cm^{-6}\ s^3$. The value m_s is actually the mass of the ion species s in AMU multiplied by 1.0453453 $x10^{-12}$ eV s^2 /AMU cm^2 . The methods used to compute the moments from this distribution will be discussed in the following sections.

3.4 Plasma Distribution Moments

In the following sections computation of the distribution moments will be discussed.

3.4.1 Ion number density (n_s)

The number density of ion species s is determined by performing the following operation on the plasma distribution array $f_{i,j,k,s}$:

$$n_s = \sum_{k=0}^{15} \Delta\alpha \sum_{i=0}^{62} \frac{v_{i+1}^3 - v_i^3}{3} \sum_{j=0}^{15} 2\sin(\bar{\beta}_j)\, sin\left(\frac{\Delta\beta}{2}\right) f_{i,j,k,s} \qquad \textbf{(15)}$$

where $\Delta\alpha$ is the azimuthal angle coverage in an acquisition period (18.25° = 0.318 radians). The velocity values v_i, v_{i+1} are determined from the energy centroids, FWHM energy passbands of the instrument, and the mass of the respective ions, m_s. $\Delta\beta$ is the measured average FWHM elevation response of the anodes, $\Delta\beta$ = 22.44° = 0.39 radians. β_j is the look direction of the jth anode from Table 5. The velocity bin size for each ion species s, at energy step i will be supplied in flight model specific spreadsheets.

With these simplifications, (15) can now be expressed in form (16):

$$n_s = 2\Delta\alpha \sin\left(\frac{\Delta\beta}{2}\right)\left[\sum_{j=0\cdots5,14,15} \frac{1}{\Lambda_j}\sin(\bar{\beta}_j) \sum_{k=0}^{15}\sum_{i=0}^{62} \frac{v_{i+1}^3 - v_i^3}{3} f_{i,(j=0\cdots5,14,15),k,s} + \sum_{j=6\cdots13} \frac{1}{\Lambda_j}\sin(\bar{\beta}_j) \sum_{i=0}^{15}\sum_{i=0}^{62} \frac{v_{i+1}^3 - v_i^3}{3} f_{i,(j=6\cdots13),k,s}\right] \qquad \textbf{(16)}$$

+

where n_s is in units of cm^{-3}. The j subscripts show that the sum is carried out over two parts j = 0-5,14,15 and j = 6-13. This is because HPCA has two sets of anodes that view azimuth spaces that are displaced 180 degrees from each other, simultaneously. Also note the inclusion of the anode coverage correction factors, Λ_j, from Table 7 included in the j summation. These will be included in all moment calculations.

3.4.2 *Ion Bulk Velocity (u_s)*

The three components of the bulk velocity of ion species s are computed from the following:

$$u_{x,s} = \frac{2}{n_s}\sin\left(\frac{\Delta\alpha}{2}\right)\times$$

$$\left[\begin{array}{c}\sum_{j=0\cdots5,14,15}\frac{1}{\Lambda_j}\left[\frac{1}{2}\Delta\beta-\frac{1}{2}\sin(\Delta\beta)\cos\left(2\bar{\beta}_j\right)\right]\sum_{k=0}^{15}\cos(\alpha_k)\sum_{i=0}^{62}\frac{v_{i+1}^4-v_i^4}{4}f_{i,(j=0\cdots5,14,15),k,s}+\\ \sum_{j=6\cdots13}\frac{1}{\Lambda_j}\left[\frac{1}{2}\Delta\beta-\frac{1}{2}\sin(\Delta\beta)\cos\left(2\bar{\beta}_j\right)\right]\sum_{k=0}^{15}\cos(\alpha_k)\sum_{i=0}^{62}\frac{v_{i+1}^4-v_i^4}{4}f_{i,(j=6\cdots13),k,s}\end{array}\right]$$

$$u_{y,s} = \frac{2}{n_s}\sin\left(\frac{\Delta\alpha}{2}\right)\times$$

$$\left[\begin{array}{c}\sum_{j=0\cdots5,14,15}\frac{1}{\Lambda_j}\left[\frac{1}{2}\Delta\beta-\frac{1}{2}\sin(\Delta\beta)\cos\left(2\bar{\beta}_j\right)\right]\sum_{k=0}^{15}\sin(\alpha_k)\sum_{i=0}^{62}\frac{v_{i+1}^4-v_i^4}{4}f_{i,(j=0\cdots5,14,15),k,s}+\\ \sum_{j=6\cdots13}\frac{1}{\Lambda_j}\left[\frac{1}{2}\Delta\beta-\frac{1}{2}\sin(\Delta\beta)\cos\left(2\bar{\beta}_j\right)\right]\sum_{k=0}^{15}\sin(\alpha_k)\sum_{i=0}^{62}\frac{v_{i+1}^4-v_i^4}{4}f_{i,(j=6\cdots13),k,s}\end{array}\right]$$

(17)

$$u_{z,s} = \frac{1}{2n_s}\Delta\alpha\,\sin(\Delta\beta)$$

$$\times\left[\sum_{j=0\cdots5,14,15}\frac{1}{\Lambda_j}\sin\left(2\bar{\beta}_j\right)\sum_{k=0}^{15}\sum_{i=0}^{62}\frac{v_{i+1}^4-v_i^4}{4}f_{i,(j=0\cdots5,14,15),k,s}\right.$$

$$\left.+\sum_{j=6\cdots13}\frac{1}{\Lambda_j}\sin\left(2\bar{\beta}_j\right)\sum_{k=0}^{15}\sum_{i=0}^{62}\frac{v_{i+1}^4-v_i^4}{4}f_{i,(j=6\cdots13),k,s}\right]$$

The vector u_s is now expressed component wise as:

$$u_s = u_{x,s}\hat{\imath} + u_{y,s}\hat{\jmath} + u_{z,s}\hat{k}$$

where $\Delta\beta$, and $\Delta\alpha$ have already been discussed. These equations result in velocity components in units of cm s^{-1}. However, they need to be reported in units of km s^{-1}. To make this conversion multiply the components by the conversion factor 1 km / 10^5 cm.

We next determine is the Scalar ion temperature.

3.4.3 *Scalar Ion Temperature*

The scalar ion temperature is determined with the following formula:

$$T_s = \left[2\Delta\alpha \frac{m_s}{3n_s} \sin\left(\frac{\Delta\beta}{2}\right) \sum_{j=0\cdots5,14,15}^{15} \frac{1}{\Lambda_j} \sin(\bar{\beta}_j) \sum_{k=0}^{15} \sum_{i=0}^{62} \frac{v_{i+1}^5 - v_i^5}{5} f_{i,0\cdots5,14,15,k,s}\right] + \left[2\Delta\alpha \frac{m_s}{3n_s} \sin\left(\frac{\Delta\beta}{2}\right) \sum_{j=6\cdots13}^{15} \frac{1}{\Lambda_j} \sin(\bar{\beta}_j) \sum_{k=0}^{15} \sum_{i=0}^{62} \frac{v_{i+1}^5 - v_i^5}{5} f_{i,j=6\cdots13,k,s}\right] - \frac{u_s^2 m_s}{3} \quad \textbf{(18)}$$

where the value of m_s is given in the following table, in units of eV s^2/cm^2. At the end of the calculation, the species specific scalar temperature is reported in eV.

Table 11: m_s values for Temperature Calculation.

Ion Species	Mass-to-Charge Ratio (M/q) [AMU/e]	m_s [eV s^2/cm^2]
H^+	1	1.04535E-12
He^{++} (alpha particle)	2	4.18138E-12
He^+	4	4.18138E-12
O^{++} (Doubly Charged Oxygen)	8	1.67255E-11
O^+	16	1.67255E-11

note that the bulk velocity, u_s, is used in (18) is of form (19):

$$\|u_s\| = \sqrt{u_{x,s}^2 + u_{y,s}^2 + u_{z,s}^2} \quad \textbf{(19)}$$

3.4.4 Ion Temperature Tensor

The ion temperature tensor is computed from the pressure tensor, P_{ij}. The nine components of the tensor are computed from:

First the diagonal terms

$$P_{xx,s} = m_s \sum_{k=0}^{15} \alpha_{k+1} - \alpha_k + \sin(\alpha_{k+1}) - \sin(\alpha_k) \sum_{i=0}^{62} \frac{v_{i+1}^5 - v_i^5}{5} - 2u_s \frac{v_{i+1}^4 - v_i^4}{4}$$
$$+ u_s^2 \frac{v_{i+1}^3 - v_i^3}{3} \sum_{j=0}^{15} \frac{1}{12} \left[\cos(3\beta_{j+1})\right.$$
$$\left. - \cos(3\beta_j) + 9\left(\cos(\beta_{j+1}) - \cos(\beta_j)\right)\right] f_{i,j,k,s}$$

To remove confusion from the subscripts, we first take note that:

$$\alpha_{k+1} - \alpha_k = \Delta\alpha$$

which is the 18.25 degrees (based on a 20 second spin period) used in previous calculations.

We can also use:

$$\sin(\alpha_{k+1}) - \sin(\alpha_k) = 2\cos\left(\frac{\alpha_{k+1}+\alpha_k}{2}\right)\sin\left(\frac{\alpha_{k+1}-\alpha_k}{2}\right) \quad \textbf{(20)}$$

Then:

$$\frac{\alpha_{k+1} + \alpha_k}{2} = \alpha_k$$

which is the midpoint of the azimuth FOV during a single energy sweep. With these substitutions $P_{xx,s}$ becomes:

$$P_{xx,s} = m_s \sum_{k=0}^{15} \frac{\Delta\alpha}{2} + \frac{1}{2}\cos(\alpha_k)\sin(\Delta\alpha) \sum_{i=0}^{62} \frac{v_{i+1}^5 - v_i^5}{5}$$
$$+ \sum_{j=0}^{15} \left[\frac{3}{2}\sin(\beta_j)\sin\left(\frac{\Delta\beta}{2}\right) - \frac{1}{6}\sin(3\beta_j)\sin\left(3\frac{\Delta\beta}{2}\right)\right] f_{i,j,k,s}$$
$$- m_s n_s u_{x,s}^2$$

Which is difficult to work with because of the sum over *k*. This can be re-expressed as:

$$p_{xx,s} = m_s \left[\sum_{j=0\cdots5,14,15}^{15} \frac{1}{\Lambda_j} \left[\frac{3}{2} \sin(\beta_j) \sin\left(\frac{\Delta\beta}{2}\right) - \frac{1}{6} \sin(3\beta_j) \sin\left(3\frac{\Delta\beta}{2}\right) \right] \sum_{k=0}^{15} \frac{\Delta\alpha}{2} \right.$$

$$+ \frac{1}{2} \cos(2\alpha_k) \sin(\Delta\alpha) \sum_{i=0}^{62} \frac{v_{i+1}^5 - v_i^5}{5} f_{i,(j=0\cdots5,14,15),k,s}$$

$$+ \sum_{j=6\cdots13}^{15} \frac{1}{\Lambda_j} \left[\frac{3}{2} \sin(\beta_j) \sin\left(\frac{\Delta\beta}{2}\right) - \frac{1}{6} \sin(3\beta_j) \sin\left(3\frac{\Delta\beta}{2}\right) \right] \sum_{k=0}^{15} \frac{\Delta\alpha}{2}$$

$$\left. + \frac{1}{2} \cos(2\alpha_k) \sin(\Delta\alpha) \sum_{i=0}^{62} \frac{v_{i+1}^5 - v_i^5}{5} f_{i,(j=6\cdots13),k,s} \right] - m_s n_s u_{x,s}^2$$

The remaining terms are much simpler to handle. Starting with $P_{yy,s}$

$$P_{yy,s} = m_s \left[\sum_{j=0\cdots5,14,15}^{15} \frac{1}{\Lambda_j} \left[\frac{3}{2} \sin(\beta_j) \sin\left(\frac{\Delta\beta}{2}\right) - \frac{1}{6} \sin(3\beta_j) \sin\left(3\frac{\Delta\beta}{2}\right) \right] \sum_{k=0}^{15} \frac{\Delta\alpha}{2} \right.$$

$$- \frac{1}{2} \cos(2\alpha_k) \sin(\Delta\alpha) \sum_{i=0}^{62} \frac{v_{i+1}^5 - v_i^5}{5} f_{i,(j=0\cdots5,14,15),k,s}$$

$$+ \sum_{j=6\cdots13}^{15} \frac{1}{\Lambda_j} \left[\frac{3}{2} \sin(\beta_j) \sin\left(\frac{\Delta\beta}{2}\right) - \frac{1}{6} \sin(3\beta_j) \sin\left(3\frac{\Delta\beta}{2}\right) \right] \sum_{k=0}^{15} \frac{\Delta\alpha}{2}$$

$$\left. - \frac{1}{2} \cos(2\alpha_k) \sin(\Delta\alpha) \sum_{i=0}^{62} \frac{v_{i+1}^5 - v_i^5}{5} f_{i,(j=6\cdots13),k,s} \right] - m_s n_s u_{y,s}^2$$

$$P_{zz,s} = m_s \Delta\alpha \left[\sum_{j=0\cdots5,14,15}^{15} \frac{1}{\Lambda_j} \left[\frac{1}{6} \sin(3\beta_j) \sin\left(3\frac{\Delta\beta}{2}\right) \right.\right.$$

$$\left. + \frac{1}{2} \sin(\beta_j) \sin\left(\frac{\Delta\beta}{2}\right) \right] \sum_{k=0}^{15} \sum_{i=0}^{62} \frac{v_{i+1}^5 - v_i^5}{5} f_{i,(j=0\cdots5,14,15),k,s}$$

$$+ \sum_{j=6\cdots13}^{15} \frac{1}{\Lambda_j} \left[\frac{1}{6} \sin(3\beta_j) \sin\left(3\frac{\Delta\beta}{2}\right) \right.$$

$$\left.\left. + \frac{1}{2} \sin(\beta_j) \sin\left(\frac{\Delta\beta}{2}\right) \right] \sum_{k=0}^{15} \sum_{i=0}^{62} \frac{v_{i+1}^5 - v_i^5}{5} f_{i,(j=6\cdots13),k,s} \right]$$

$$- m_s n_s u_{z,s}^2$$

Now the off diagonal terms with some degeneracy:

$$P_{xy,s} = m_s \left[\sum_{j=0\cdots5,14,15}^{15} \frac{1}{\Lambda_j} \left[\frac{3}{2} \sin(\beta_j) \sin\left(\frac{\Delta\beta}{2}\right) \right.\right.$$

$$\left. - \frac{1}{6} \sin(3\beta_j) \sin\left(3\frac{\Delta\beta}{2}\right) \right] \sum_{k=0}^{15} \left[\frac{1}{2} \sin(2\alpha_k) \sin(\Delta\alpha) \right] \sum_{i=0}^{62} \frac{v_{i+1}^5 - v_i^5}{5} f_{i,(j=0\cdots5,14,15),k,s}$$

$$+ \sum_{j=6\cdots13}^{15} \frac{1}{\Lambda_j} \left[\frac{3}{2} \sin(\beta_j) \sin\left(\frac{\Delta\beta}{2}\right) \right.$$

$$\left.\left. - \frac{1}{6} \sin(3\beta_j) \sin\left(3\frac{\Delta\beta}{2}\right) \right] \sum_{k=0}^{15} \left[\frac{1}{2} \sin(2\alpha_k) \sin(\Delta\alpha) \right] \sum_{i=0}^{62} \frac{v_{i+1}^5 - v_i^5}{5} f_{i,(j=6\cdots13),k,s} \right]$$

$$- m_s n_s u_{x,s} u_{y,s}$$

$$P_{yx,s} = P_{xy,s}$$

$$P_{xz,s} = m_s \left[\sum_{j=0\cdots5,14,15}^{15} \frac{1}{\Lambda_j} \left[\frac{1}{2} \cos(\beta_j) \sin\left(\frac{\Delta\beta}{2}\right) \right.\right.$$

$$\left. - \frac{1}{6} \cos(3\beta_j) \sin\left(3\frac{\Delta\beta}{2}\right) \right] \sum_{k=0}^{15} \left[2\cos(\alpha_k) \sin\left(\frac{\Delta\alpha}{2}\right) \right] \sum_{i=0}^{62} \frac{v_{i+1}^5 - v_i^5}{5} f_{i,(j=0\cdots5,14,15),k,s}$$

$$+ \sum_{j=6\cdots13}^{15} \frac{1}{\Lambda_j} \left[\frac{3}{2} \sin(\beta_j) \sin\left(\frac{\Delta\beta}{2}\right) \right.$$

$$\left.\left. - \frac{1}{6} \sin(3\beta_j) \sin\left(3\frac{\Delta\beta}{2}\right) \right] \sum_{k=0}^{15} \left[2\cos(\alpha_k) \sin\left(\frac{\Delta\alpha}{2}\right) \right] \sum_{i=0}^{62} \frac{v_{i+1}^5 - v_i^5}{5} f_{i,(j=6\cdots13),k,s} \right]$$

$$- m_s n_s u_{x,s} u_{z,s}$$

$$P_{zx,s} = P_{xz,s}$$

$$
\begin{aligned}
&P_{yz,s} \\
&= m_s \Bigg[\sum_{j=0\cdots5,14,15}^{15} \frac{1}{\Lambda_j} \Big[\frac{1}{2} \cos(\beta_j) \sin\left(\frac{\Delta\beta}{2}\right) \\
&- \frac{1}{6} \cos(3\beta_j) \sin\left(\frac{3\Delta\beta}{2}\right) \Big] \sum_{k=0}^{15} \Big[2 \sin(\alpha_k) \sin\left(\frac{\Delta\alpha}{2}\right) \Big] \sum_{i=0}^{62} \frac{v_{i+1}^5 - v_i^5}{5} f_{i,(j=0\cdots5,14,15),k,s} \\
&+ \sum_{j=6\cdots13}^{15} \frac{1}{\Lambda_j} \Big[\frac{1}{2} \cos(\beta_j) \sin\left(\frac{\Delta\beta}{2}\right) \\
&- \frac{1}{6} \cos(3\beta_j) \sin\left(\frac{3\Delta\beta}{2}\right) \Big] \sum_{k=0}^{15} \Big[2 \sin(\alpha_k) \sin\left(\frac{\Delta\alpha}{2}\right) \Big] \sum_{i=0}^{62} \frac{v_{i+1}^5 - v_i^5}{5} f_{i,(j=6\cdots13),k,s} \Bigg] \\
&- m_s n_s u_{y,s} u_{z,s}
\end{aligned}
$$

$$P_{zy,s} = P_{yz,s}$$

With the Pressure tensor Expressed as:

$$P_s = \begin{bmatrix} P_{xx,s} & P_{yx,s} & P_{zx,s} \\ P_{xy,s} & P_{yy,s} & P_{zy,s} \\ P_{xz,s} & P_{yz,s} & P_{zz,s} \end{bmatrix}$$

Where the units of pressure are eV/cm3; 1 eV/cm3 = 1.602e-4 nanopascals

To diagonalize the tensor we use the algorithm devised by Joachim Kopp [2008].
When diagonalized, P has the form:

$$P_s = \begin{bmatrix} P'_{xx,s} & 0 & 0 \\ 0 & P'_{yy,s} & 0 \\ 0 & 0 & P'_{zz,s} \end{bmatrix}$$

where ' indicates the component following diagonalization

From the diagonalized form of the pressure tensor, we then determine T_s from:

$$T_s = \frac{P'_s}{n_s}$$

Where n_s is the number density of ion species s determined previously.

4. Data Products with RF

When computing flux with RF, multiply the counts for ion species s by the values specific to the energy step and ion species. This needs to be done for energy steps 36 - 49 (14 steps in all). Three RF tables are going to be used: one which attenuates proton flux by 50%, one that attenuates 90%, and one more that decreases proton flux by a 99%. The computation for the flux is then:

$$J_{i,j,k,s} = \frac{C_{i,j,k,s}\varepsilon_i}{G_j(E_i)\,E_i} \qquad \textbf{(21)}$$

Where ε_i is the attenuation correction from one of the 3 tables. Calculations of f(v) and moments follow directly from these values.

5. Level 2 Data Products: In the magnetic field reference frame

HPCA data products and moments are computed in the spacecraft reference frame using the magnetic field data acquired with the magnetometer probes on each of the spacecraft. Scalar moments, such as the number density and scalar temperature require no transformation. The remainder of this section will focus on the values which do; bulk velocity, and the pressure/temperature tensor.

5.1 Bulk velocity in the Magnetic Field Frame

Transforming the bulk velocity into the magnetic field frame requires that we first determine a magnetic field unit vector:

$$\hat{\mathrm{b}} = \frac{\vec{B}}{\|B\|} = \frac{B_x\hat{\imath} + B_y\hat{\jmath} + B_z\hat{k}}{\sqrt{B_x^2 + B_y^2 + B_z^2}} \tag{22}$$

Once b is determined, the magnitude of the bulk velocity of species s in the direction of the magnetic field is:

$$V_{\|,s} = \vec{u}_s \cdot \hat{b} = u_{x,s}b_x + u_{y,s}y + u_{z,s}b_z \tag{23}$$

and the velocity vector of the ion species, parallel to the magnetic field (v-parallel) is then:

$$\vec{V}_{\|,s} = V_{\|,s}\hat{b} = V_{\|,s}b_x\hat{\imath} + V_{\|,s}y\,\hat{\jmath} + V_{\|,s}b_z\hat{k} \tag{24}$$

Once found, we can then use the parallel velocity vector to find the velocity vector perpendicular to the magnetic field (v-perpendicular):

$$\vec{V}_{\perp,s} = \vec{u}_s - \vec{V}_{\|,s} = \left(u_{x,s} - V_{\|x,s}\right)\hat{\imath} + \left(u_{y,s} - V_{\|y,s}\right)\hat{\jmath} + \left(u_{z,s} - V_{\|z,s}\right)\hat{k} \tag{25}$$

In addition to computing the velocity components which are parallel, and perpendicular to the magnetic field, the pressure tensor needs to be transformed into the magnetic field frame using the following:

TBD

Once all of the moments of the plasma distribution are transformed into the magnetic field frame, we can then begin constructing a second velocity distribution function which is also transformed into the magnetic field frame.

5.2 f(v) in the Field aligned coordinates

Expressing the velocity distribution function in the magnetic field frame involves a translation in velocity, and a rotation. For each bin f_{ijk} in the discretized distribution function (remember that 16 adjacent azimuths/full energy sweeps constitute a full-sky observation) there will be three vector components associated with that bin, that represent the velocity relative to a component system in which the magnetic field is directed in the positive z direction. The vector components in translated into the magnetic field frame (the primed coordinate system) are determined from the base system (unprimed system) with the following:

$$\begin{aligned}\vec{v}'_{ijk,s} = \vec{v}_{ijks} - \vec{V}_{\perp,H^+} \\ &= \left(v_{x,ijk,s} - V_{\perp x,H^+}\right)\hat{\imath} + \left(v_{y,ijk,s} - V_{\perp y,H^+}\right)\hat{\jmath} \\ &+ \left(v_{z,ijk,s} - V_{\perp z,H^+}\right)\hat{k}\end{aligned} \quad \textbf{(26)}$$

where $v_{x,ijk,s}$ is:

$$v_{x,ijk,s} = \sqrt{\frac{2E_i}{m_s}}\sin(\beta_j)\cos(\alpha_k) \quad \textbf{(27)}$$

$v_{y,ijk,s}$ is:

$$v_{y,ijk,s} = \sqrt{\frac{2E_i}{m_s}}\sin(\beta_j)\sin(\alpha_k) \quad \textbf{(28)}$$

and:

$$v_{z,ijk,s} = \sqrt{\frac{2E_i}{m_s}}\cos(\beta_j) \quad \textbf{(29)}$$

Each primed velocity value is computed on a bin-by-bin basis. The energies E_i are instrument specific and based on the voltage at each step with the analyzer constants from Table 1. The ms values are found in Table 11. For instance, $f_{000,H+}$ will be accompanied by values of:

$$v'_{x,000,H^=} = \sqrt{\frac{2E_0}{m_s}}\sin(123.75°)\cos(180°) - \left(u_{x,H^+} - V_{\parallel x,H^+}\right) \quad \textbf{(30)}$$

$$v'_{y,000,H^{=}} = \sqrt{\frac{2E_0}{m_s}}\sin(123.75°)\sin(180°) - \left(u_{y,H^+} - V_{\|y,H^+}\right) \quad \textbf{(31)}$$

$$v'_{z,000,H^{=}} = \sqrt{\frac{2E_0}{m_s}}\cos(123.75°) - \left(u_{z,H^+} - V_{\|z,H^+}\right) \quad \textbf{(32)}$$

and so on, until all 64 velocities, 16 elevation, and 16 azimuths are accounted for.

In addition to the velocity translation, the coordinate system must be rotated such that the magnetic field is in the direction of the +Z axis. The unit vectors of this coordinate system are:

$$\hat{X}_s = \frac{(\hat{b}\times \vec{u}_s)\times\hat{b}}{\|\vec{u}_s\|} = \frac{\begin{aligned}&\left[-(b_x u_z - u_x b_z)b_z - \left(b_x u_y - u_x b_y\right)b_y\right]\hat{\imath}\\ &+\left[\left(b_y u_z - u_y b_z\right)b_z - \left(b_x u_y - u_x b_y\right)b_x\right]\hat{\jmath}\\ &+\left[\left(b_y u_z - u_y b_z\right)b_y - (b_x u_z - u_x b_z)b_x\right]\hat{k}\end{aligned}}{\|\vec{u}_s\|} \quad \textbf{(33)}$$

$$\hat{Y}_s = \frac{(\hat{b}\times \vec{u}_s)}{\|\vec{u}_s\|} = \frac{\left(b_y u_{z,s} - b_z u_{y,s}\right)\hat{\imath} - \left(b_x u_{z,s} - b_z u_{x,s}\right)\hat{\jmath} + \left(b_x u_{y,s} - b_y u_{x,s}\right)\hat{k}}{\|\vec{u}_s\|} \quad \textbf{(34)}$$

$$\hat{Z}_s = \hat{\mathrm{b}} = \frac{B_x\hat{\imath} + B_y\hat{\jmath} + B_z\hat{k}}{\sqrt{B_x^2 + B_y^2 + B_z^2}} = b_x\hat{\imath} + b\hat{\jmath} + z_z\hat{k} \quad \textbf{(35)}$$

With the vector so determined, rotation matrix is:

$$T = \begin{bmatrix} \frac{\left[-(b_x u_z - u_x b_z)b_z - \left(b_x u_y - u_x b_y\right)b_y\right]}{\|\vec{u}_s\|} & \frac{\left[\left(b_y u_z - u_y b_z\right)b_z - \left(b_x u_y - u_x b_y\right)b_x\right]}{\|\vec{u}_s\|} & \frac{\left[\left(b_y u_z - u_y b_z\right)b_z - \left(b_x u_y - u_x b_y\right)b_x\right]}{\|\vec{u}_s\|} \\ \frac{\left(b_y u_{z,s} - b_z u_{y,s}\right)}{\|\vec{u}_s\|} & \frac{\left(b_x u_{z,s} - b_z u_{x,s}\right)}{\|\vec{u}_s\|} & \frac{\left(b_x u_{y,s} - b_y u_{x,s}\right)}{\|\vec{u}_s\|}/\|\vec{u}_s\| \\ b_x & b_y & b_z \end{bmatrix} \quad \textbf{(36)}$$

And the matrix used to rotate the velocity components in the field aligned coordinate system is the transpose of this matrix

$$T^t = \begin{bmatrix} \frac{\left[-(b_x u_z - u_x b_z) b_z - (b_x u_y - u_x b_y) b_y\right]}{\|\vec{u}_s\|} & \frac{(b_y u_{z,s} - b_z u_{y,s})}{\|\vec{u}_s\|} & b_x \\ \frac{\left[(b_y u_z - u_y b_z) b_z - (b_x u_y - u_x b_y) b_x\right]}{\|\vec{u}_s\|} & \frac{(b_x u_{z,s} - b_z u_{x,s})}{\|\vec{u}_s\|} & b_y \\ \frac{\left[(b_y u_z - u_y b_z) b_y - (b_x u_z - u_x b_z) b_x\right]}{\|\vec{u}_s\|} & \frac{(b_x u_{y,s} - b_y u_{x,s})}{\|\vec{u}_s\|} & b_z \end{bmatrix} \quad \textbf{(37)}$$

With the operation:

$$\overrightarrow{v''}_s = T^t \overrightarrow{v'}_s \quad \textbf{(38)}$$

From the primed coordinates in equation 6.

6. Appendix 1- Re-evaluation of Effective Area based on Instrument Flux Measurements

Discrepancies in moment calculations (particularly number density) were discovered in August 2015. These discrepancies were traced to errors in beam current measurement during calibration. Once this was realized, the research team began inspecting magnetosheath data at the highest resolution (fast survey) to determine the inter-instrument correction factors, assuming MMS1-HPCA is accurate. The distance between the spacecraft was negligible over the time space for this data, so the flux seen by each instrument is essentially the same. The data for each instrument was averaged over the time interval into count arrays of 64 energies by 16 elevation anodes. The expression for flux (13) was used, with G expanded into the form shown in (11). With equal fluxes, and the other values accounted for, the correction values were found by solving $A_{0(FMk)} = C_k A_{0(FM1)}$, where k = 2, 3, or 4. The following table, determined from this analysis, replaces Table 9.

Table 12: Updated A_0's

Voltage Step (i)	A_0 FM 1 (cm^2)	A_0 FM 2 (cm^2)	A_0 FM 3 (cm^2)	A_0 FM 4 (cm^2)
0	0.025	0.021	0.023	0.024

1	0.025	0.021	0.023	0.024
2	0.026	0.022	0.024	0.025
3	0.026	0.022	0.024	0.025
4	0.026	0.022	0.024	0.025
5	0.027	0.023	0.025	0.026
6	0.027	0.023	0.025	0.026
7	0.028	0.024	0.025	0.027
8	0.028	0.024	0.025	0.027
9	0.029	0.024	0.026	0.028
10	0.029	0.024	0.026	0.028
11	0.03	0.025	0.027	0.029
12	0.03	0.025	0.027	0.029
13	0.031	0.026	0.028	0.029
14	0.031	0.026	0.028	0.029
15	0.032	0.027	0.029	0.030
16	0.032	0.027	0.029	0.030
17	0.033	0.028	0.030	0.031
18	0.033	0.028	0.030	0.031
19	0.034	0.029	0.031	0.032
20	0.035	0.029	0.032	0.033
21	0.035	0.029	0.032	0.033
22	0.036	0.030	0.033	0.034
23	0.036	0.030	0.033	0.034
24	0.037	0.031	0.034	0.035
25	0.037	0.031	0.034	0.035
26	0.038	0.032	0.035	0.036
27	0.039	0.033	0.035	0.037
28	0.039	0.033	0.035	0.037
29	0.04	0.034	0.036	0.038
30	0.041	0.035	0.037	0.039

31	0.041	0.035	0.037	0.039
32	0.042	0.035	0.038	0.040
33	0.043	0.036	0.039	0.041
34	0.043	0.036	0.039	0.041
35	0.044	0.037	0.040	0.042
36	0.045	0.038	0.041	0.043
37	0.046	0.039	0.042	0.044
38	0.046	0.039	0.042	0.044
39	0.047	0.040	0.043	0.045
40	0.048	0.040	0.044	0.046
41	0.049	0.041	0.045	0.047
42	0.05	0.042	0.046	0.048
43	0.05	0.042	0.046	0.048
44	0.051	0.043	0.046	0.048
45	0.052	0.044	0.047	0.049
46	0.053	0.045	0.048	0.050
47	0.054	0.045	0.049	0.051
48	0.055	0.046	0.050	0.052
49	0.056	0.047	0.051	0.053
50	0.057	0.048	0.052	0.054
51	0.058	0.049	0.053	0.055
52	0.059	0.050	0.054	0.056
53	0.06	0.051	0.055	0.057
54	0.06	0.051	0.055	0.057
55	0.062	0.052	0.056	0.059
56	0.063	0.053	0.057	0.060
57	0.064	0.054	0.058	0.061
58	0.068	0.057	0.062	0.065
59	0.066	0.056	0.060	0.063
60	0.063	0.053	0.057	0.060

61	0.061	0.051	0.056	0.058
62	0.057	0.048	0.052	0.054
63	0	0.000	0.000	0.000

7. Appendix-2 Table of HPCA Specific Level 2 Parameter Values and units

Variable Name in L2 **ion** files, where X = 1,2,3,4 dependent on the MMS spacecraft	Units of Measure – if empty, variable is unitless
Epoch	ns
Epoch_MINUS	ms
Epoch_PLUS	ms
mmsX_hpca_polar_anode_number	
mmsX_hpca_azimuth_decimation_factor	
mmsX_hpca_polar_decimation_factor	
mmsX_hpca_energy_decimation_factor	
mmsX_hpca_sweep_table_number	
mmsX_hpca_start_azimuth	
mmsX_hpca_science_mode	
mmsX_hpca_ion_energy	eV
mmsX_hpca_hplus_flux	1/(cm^2 s sr eV)
mmsX_hpca_hplus_phase_space_density	cm^-6 s^3
mmsX_hpca_hplus_data_quality	Data_Quality_Key global attribute
mmsX_hpca_heplus_flux	1/(cm^2 s sr eV)
mmsX_hpca_heplus_phase_space_density	cm^-6 s^3
mmsX_hpca_heplus_data_quality	Data_Quality_Key global attribute
mmsX_hpca_heplusplus_flux	1/(cm^2 s sr eV)
mmsX_hpca_heplusplus_phase_space_density	cm^-6 s^3
mmsX_hpca_heplusplus_data_quality	Data_Quality_Key global attribute

mmsX_hpca_oplus_flux	1/(cm^2 s sr eV)
mmsX_hpca_oplus_phase_space_density	cm^-6 s^3
mmsX_hpca_oplus_data_quality	Data_Quality_Key global attribute
mmsX_hpca_B_GSE_sweep_avg	nT
mmsX_hpca_B_GSM_sweep_avg	nT
Epoch_Angles	Ns
Epoch_MINUS_Angles	Ms
Epoch_PLUS_Angles	Ms
mmsX_hpca_azimuth_angles_degrees	Deg
mmsX_hpca_azimuth_angles_per_ev_degrees	Deg
mmsX_hpca_centroid_elevation_angle	Deg
mmsX_hpca_azimuth_index	
mmsX_hpca_energy_step_number	
Global Attribute: Data_Quality_Key	0: Bad 1: Good 2: Good, RF on, Bkgd on 3: Good, RF off, Bkgd on 4: Good, RF on, Bkgd off 5: Good, RF off, Bkgd off 6: Good, Non-sweeping data

Variable Name in L2 **moments** files, where X = 1,2,3,4 dependent on the MMS spacecraft	Units of Measure – if empty, variable is unitless
Epoch	Ns
Epoch_MINUS	Ms
Epoch_PLUS	Ms
mmsX_hpca_spin_number	
mmsX_hpca_ion_energy	eV
mmsX_hpca_sweep_table_number	
mmsX_hpca_science_mode	
mmsX_hpca_hplus_number_density	cm^-3

mmsX_hpca_hplus_ion_bulk_velocity	km/s
mmsX_hpca_hplus_scalar_temperature	eV
mmsX_hpca_hplus_ion_pressure	nPa
mmsX_hpca_hplus_temperature_tensor	eV
mmsX_hpca_heplus_number_density	cm^-3
mmsX_hpca_heplus_ion_bulk_velocity	km/s
mmsX_hpca_heplus_scalar_temperature	eV
mmsX_hpca_heplus_ion_pressure	nPa
mmsX_hpca_heplus_temperature_tensor	eV
mmsX_hpca_heplusplus_number_density	cm^-3
mmsX_hpca_heplusplus_ion_bulk_velocity	km/s
mmsX_hpca_heplusplus_scalar_temperature	eV
mmsX_hpca_heplusplus_ion_pressure	nPa
mmsX_hpca_heplusplus_temperature_tensor	eV
mmsX_hpca_oplus_number_density	cm^-3
mmsX_hpca_oplus_ion_bulk_velocity	km/s
mmsX_hpca_oplus_scalar_temperature	eV
mmsX_hpca_oplus_ion_pressure	nPa
mmsX_hpca_oplus_temperature_tensor	eV
mmsX_hpca_B_GSE_spin_avg	nT
mmsX_hpca_B_GSM_spin_avg	nT
mmsX_hpca_hplus_ion_bulk_velocity_GSM	km/s
mmsX_hpca_hplus_tperp	eV
mmsX_hpca_hplus_tparallel	eV
mmsX_hpca_hplus_vperp	km/s
mmsX_hpca_hplus_vparallel	km/s
mmsX_hpca_hplus_vperp_GSM	km/s
mmsX_hpca_hplus_vparallel_GSM	km/s
mmsX_hpca_heplus_ion_bulk_velocity_GSM	km/s
mmsX_hpca_heplus_tperp	eV
mmsX_hpca_heplus_tparallel	eV
mmsX_hpca_heplus_vperp	km/s
mmsX_hpca_heplus_vparallel	km/s

mmsX_hpca_heplus_vperp_GSM	km/s
mmsX_hpca_heplus_vparallel_GSM	km/s
mmsX_hpca_heplusplus_ion_bulk_velocity_GSM	km/s
mmsX_hpca_heplusplus_tperp	eV
mmsX_hpca_heplusplus_tparallel	eV
mmsX_hpca_heplusplus_vperp	km/s
mmsX_hpca_heplusplus_vparallel	km/s
mmsX_hpca_heplusplus_vperp_GSM	km/s
mmsX_hpca_heplusplus_vparallel_GSM	km/s
mmsX_hpca_oplus_ion_bulk_velocity_GSM	km/s
mmsX_hpca_oplus_tperp	eV
mmsX_hpca_oplus_tparallel	eV
mmsX_hpca_oplus_vperp	km/s
mmsX_hpca_oplus_vparallel	km/s
mmsX_hpca_oplus_vperp_GSM	km/s
mmsX_hpca_oplus_vparallel_GSM	km/s
Global Attribute: Data_Quality_Key	0: Bad 1: Good 2: Good, RF on, Bkgd on 3: Good, RF off, Bkgd on 4: Good, RF on, Bkgd off 5: Good, RF off, Bkgd off 6: Good, Non-sweeping data